07

Schottky diodes based on monocrystalline Al/AlGaN/GaN heterostructures for zero-bias microwave detection

© N.V. Vostokov,¶ M.N. Drozdov, M.A. Kalinnikov, S.A. Kraev, D.N. Lobanov, P.A. Yunin

Institute for Physics of Microstructures of the Russian Academy of Sciences, Nizhny Novgorod 603950, Russia
¶e-mail: vostokov@ipm.sci-nnov.ru

Received April 27, 2024
Revised December 30, 2025
Accepted February 11, 2025

The microwave properties of novel all-epitaxial Al/AlGaN/GaN low-barrier Schottky diodes with near-surface polarization-induced δ-doping are studied. An original technique for on-wafer microwave measurements of test structures is used. The possibility of development of a highly sensitive zero-bias microwave detector based on a planar low-barrier metal-semiconductor-metal heterostructure, which does not require the formation of ohmic contact of the semiconductor with the metal, is demonstrated. Estimates show that the cutoff frequency of such a detector can reach approximately 100 GHz for relevant values of the detecting contact area $\sim 10\,\mu\text{m}^2$.

Keywords: low-barrier GaN Schottky diode, on-wafer microwave measurements, structural defects and trap states in a semiconductor, zero-bias microwave detector

DOI: 10.61011/TP.2025.06.61378.151-24

Introduction

Mastering the microwave-terahertz frequency range of the electromagnetic spectrum requires the creation of convenient and compact solid-state devices for detecting, mixing, and rectifying signals. The most common nonlinear elements in uncooled receivers and RF/DC converters of microwave-terahertz radiation are Schottky (Mott) barrier diodes [1,2]. Diodes are widely used in mixing and rectifying circuits. Somewhat less frequently, Schottky diodes are used as quadratic and video detectors [3]. To ensure high detection sensitivity, diodes with a reduced effective Schottky barrier height are required to eliminate the need for a constant bias. This simplifies the receiver design and results in lower noise levels due to the absence of DC bias current. An example is low-barrier Mott diodes based on GaAs with near-surface isotype δ-doping [4,5]. In the mixing mode of operation, reducing the effective height of the diode barrier makes it possible to decrease the required local-oscillator power level [6,7], and in the rectifier mode this increases the efficiency of RF/DC conversion for a low power of the microwave signal [8,9]. Other types of nonlinear elements that operate without constant bias are also being developed. These include planar doped barrier diodes [10], diodes based on InAs/AlSb/AlGaSb heterostructures with interband tunneling [11], resonant tunnel diodes based on AlAs/InGaAs/InAs [12], asymmetric spacer tunnel layer diodes [13], semimetal/semiconductor diodes [14], InP/InGaAs heterobarrier diodes [15], heterostructure diodes with AlGaInAs graded-gap barrier [16], InGaAs/AlGaAs/GaAs heterobarrier diodes [17], self-switching diodes [18], lateral diodes [19], FETs [20], etc.

The specificity of wide-gap nitrides lies in the possibility of creating devices operating at high power densities and temperatures, exposure to radiation, and in aggressive environments [21]. The unique characteristics of these materials are due to the high binding energy of the atoms in the crystal lattice and the wide band gap. At the same time, this makes it difficult to create low emission barriers. There is little research on zero-bias GaN diodes. A few examples include self-switching [18] and lateral [19] diodes. Note that both types of devices, although called diodes, use the transistor detection principle. Another distinctive feature of wide-gap nitride semiconductors is the record values of spontaneous polarization and the piezoelectric tensor component. Strong polarization effects can be used as an additional degree of freedom in the development of device heterostructures based on these materials [22]. Our recent papers [23,24] demonstrated the possibility of reducing the effective height of the Schottky (Mott) barrier in a metal/AlGaN/GaN heterostructure with Ga-face polarity due to polarization-induced δ-doping of the AlGaN/GaN heterojunction. A positive polarization charge located in the plane of the AlGaN/GaN heterointerface forms a potential profile with a tunnel-transparent trapezoidal barrier at the interface with the metal, which reduces the effective height of the diode barrier. In Ref. 24 all-epitaxial Al/AlGaN/GaN low-barrier Schottky diodes with high values of low-frequency ampere-watt sensitivity $\alpha = -(\mathrm{d}R/\mathrm{d}U)/(2R)$ and low specific value of differential resistance R at zero bias U were fabricated using molecular beam epitaxy (MBE). This paper stud-

ies the impedance and detection characteristics of such diodes in the microwave range. The impact of structural defects, the high density of which is typical of nitride heterostructures grown on lattice-mismatched substrates, is studied.

1. Description of diode structures and measurement techniques

Diode heterostructures were grown by MBE with nitrogen plasma activation in an STE 3N3 (SemiTEq) setup with an HD25 active nitrogen source (Oxford Applied Research). Two-inch sapphire wafers with the c (0001) plane oriented parallel to the wafer surface were used as substrates. After the formation of the buffer layers, a contact layer of n^+-GaN 1 μm thick and heavily doped with donors (Si) was grown. A nominally undoped GaN barrier layer 120 nm thick was then grown, followed by an undoped $Al_xGa_{1-x}N$ layer 1 nm thick. At the end of the growing process, to create a Schottky barrier, an epitaxial single-crystal metal layer of Al 70 nm thick was formed from the same effusion cell that was used when the semiconductor part of the heterostructure was grown. The chemical composition of heterostructures was analyzed by secondary-ion mass spectrometry using a TOF.SIMS-5 (IONTOF) setup. X-ray diffraction measurements were performed using a Bruker D8 Discover X-ray diffractometer. The fabrication process and diagnostic methods of heterostructures are described in more detail in Ref. 24. Figure 1 shows schematically the depth-dependence of the position of the bottom of the conduction band and the position of the Fermi level in a low-barrier diode heterostructure [23,24]. Two low-barrier diode heterostructures D1 and D2 with a similar composition of the $Al_xGa_{1-x}N$ solid solution ($x \approx 0.6$) were studied. Diode heterostructure D3 without an $Al_xGa_{1-x}N$ layer, namely, a conventional Al/GaN Schottky diode with a standard barrier height, was also examined for comparison. The doping level of the n^+-GaN contact layer in diode heterostructures D1–D3 was $1.2 \times 10^{19}\,cm^{-3}$, $2 \times 10^{19}\,cm^{-3}$, and $3 \times 10^{18}\,cm^{-3}$, respectively.

To explore the microwave properties of diodes, we used the approach that we had previously employed to study various electrophysical characteristics of diode and transistor heterostructures on a growth plate [17,25]. Test planar diode structures, representing two back-to-back Schottky contacts, separated from each other by an annular gap free of metallization, with inner and outer radii a and b, respectively, were fabricated. Structures with $a = 10\,\mu$m and $b = 20\,\mu$m were used for the measurements. When test structures were formed, additional metal layers of Au/Ni (100 nm/50 nm) were deposited on the samples on top of the Al layer using electron beam evaporation. A scheme of the layers sequence of the test diode structure is shown in the inset to Fig. 1. To perform microwave measurements, the test structures were connected to an E8361A Vector Network Analyzer (VNA) (Agilent Technologies) using a

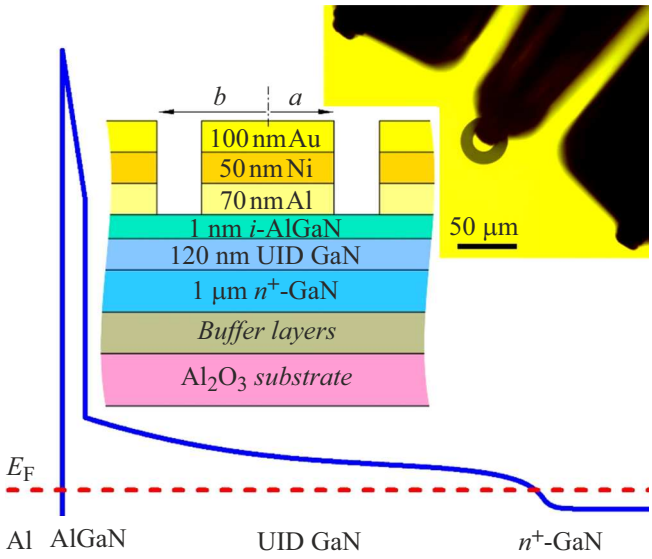

Figure 1. Band diagram of a low-barrier diode heterostructure. The inset shows a scheme of the layers sequence in the test diode structure and a photograph of the test structure in contact with the microwave probe.

microwave probe (Cascade Microtech), as shown in the photograph in the inset to Fig. 1. A DC voltage source for measuring the dependence of the diode parameters on the bias and a voltmeter for measuring the detected voltage were connected to the structures through a low-frequency circuit built into the VNA, decoupled from the microwave path. The impedance spectra of the structures $Z_m = Z_0(1 + S_{11})/(1 - S_{11})$ ($Z_0 = 50\,\Omega$) were determined from the measured frequency dependences of the reflectivity of the probing signal S_{11}. The reflectivity was measured in the frequency range $f = 0.01 - 67$ GHz (1600 frequencies distributed over the range with a logarithmic step) for the power level -20 dBm of the microwave signal generated by the VNA. Before measurements, single-port calibration of the analyzer and microwave path was performed using a standard set of calibration measures. To determine the unknown parameters of the diode heterostructure, we introduced the residual function

$$\Phi = \sum_f \left\{ \left[\frac{\mathrm{Re}(Z_m - Z)}{\mathrm{Re}(Z_m)} \right]^2 + \left[\frac{\mathrm{Im}(Z_m - Z)}{\mathrm{Im}(Z_m)} \right]^2 \right\}, \qquad (1)$$

where the summation is carried out over all frequencies at which impedance measurements were performed. Function Φ characterizes the relative deviation of the model impedance value Z of the test diode structure from the experimental value Z_m. The desired values of the unknown parameters of the heterostructure were taken to be those values that minimized the residual function. The Φ minimization procedure was performed in the frequency range $f = 0.05 - 50$ GHz. The impedance of the test structure can be represented as the sum $Z = Z_i + Z_e + R_r$. Here, Z_i is the impedance of the internal

distributed Schottky contact, Z_e is the impedance of the external distributed contact, $R_r = (\rho_r/2\pi)\ln(b/a)$ is the resistance of the annular semiconductor region with sheet resistance ρ_r located between the internal and external contacts. The problem of the impedance of distributed metal-semiconductor contacts of various shapes has been considered many times in the literature [26,27]. The solution is based on representing the contact as a transmission line with a small-signal propagation constant $\gamma = (\rho g)^{1/2}$, where g is the admittance per unit area of the transition between the metal and the semiconductor, ρ is the sheet resistance of the semiconductor under the metal. For the structures under study, with a high degree of accuracy, $\rho = \rho_r$ and is determined by the sheet resistance of the heavily doped contact layer. It is assumed that the drop in DC voltage across the non-depleted region of the semiconductor can be neglected; therefore, γ is coordinate independent. Taking this into account, the impedances of the internal and external distributed contacts of the test structure are determined by the expressions [25,27]

$$Z_i = \frac{\rho}{2\pi\gamma a}\frac{I_0(\gamma a)}{I_1(\gamma a)}, \tag{2}$$

$$Z_e = \frac{\rho}{2\pi\gamma b}\frac{K_0(\gamma b)}{K_1(\gamma b)}, \tag{3}$$

where I_n and K_n are modified Bessel functions of order n. When the dependences of the parameters of diode heterostructures on the DC bias voltage were measured, the internal contact of the test structure was the measuring one. For reverse and small forward biases of the internal contact, the DC voltage drop on the external contact can be neglected due to its significantly larger area. This also makes it possible to use test structures for measuring static $I-V$ characteristics of the diodes. The $I-V$ characteristics of low-barrier diodes D1 and D2 were measured on the same test structures on which the microwave measurements were carried out. The $I-V$ characteristic of the diode heterostructure D3 was measured on a separate sample using a Schottky contact with a diameter of 10 μm and an ohmic contact formed by fusing a drop of indium deposited on the surface of a semiconductor. Static $I-V$ characteristics were measured using a 4200-SCS parametric analyzer (Keithley Instruments). When studying the detection characteristics, the internal contact of the test structure was the detecting one, and the external one played the role of an ohmic contact. It follows from the calculations based on the results of the measurements that in the frequency range we used, the radius of the internal contact is less than the characteristic length $|\gamma|^{-1}$ of current flow into it; therefore, the contact behaves as a nonlinear one with lumped parameters. Since $\mathrm{Re}\,Z_i \gg \mathrm{Re}\,Z_e$, much more power is absorbed in the internal contact than in the external one. Moreover, the nonlinear properties of the external contact are greatly suppressed because its dimensions are much larger than $|\gamma|^{-1}$ [27]. For these reasons, the detecting properties of the external contact can be neglected. The volt-watt sensitivity of the test diode structures was measured without supplying an external bias at several fixed frequencies at the power level -20 dBm of the microwave signal generated by the VNA. The detected voltage was measured using a 34401A multimeter (Agilent Technologies). Measuring the reflectivity of the microwave signal from the diode structure together with calibration measurements made it possible to determine the power absorbed in the structure.

2. Results and discussion

Static $I-V$ characteristics and dependences of specific differential resistance and low-frequency ampere-watt sensitivity on voltage for the diode structures under study are shown in Fig. 2. The dependences $R(U)$ and $\alpha(U)$ were obtained by numerical differentiation of the measured $I-V$

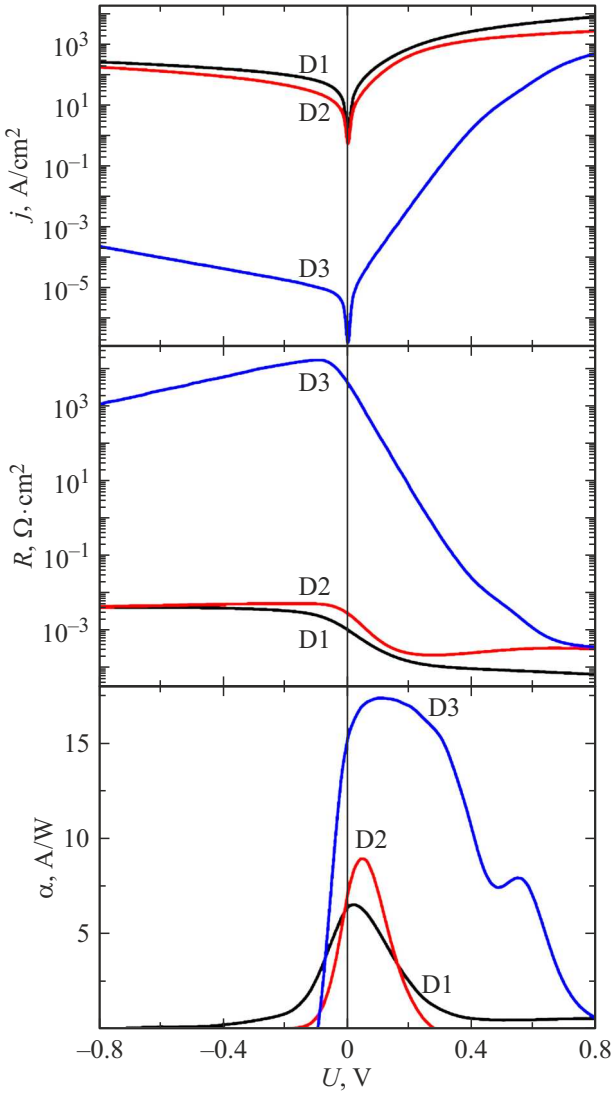

Figure 2. Static $I-V$ characteristics and dependences of specific differential resistance and low-frequency ampere-watt sensitivity on voltage for the studied diode structures.

Diode parameters.

Name of diodes	D1	D2	D3
R at zero bias, $\Omega \cdot \mathrm{cm}^2$	9.7×10^{-4}	2.7×10^{-3}	3800
α at zero bias, A/W	6.4	7.2	15.4
R_b at zero bias, $\Omega \cdot \mathrm{cm}^2$	9.2×10^{-4}	2.5×10^{-3}	
C_b at zero bias, F/cm^2	9.9×10^{-8}	1.08×10^{-7}	7.8×10^{-8}
l_d at zero bias, nm	93	85	118
r at zero bias, $\Omega \cdot \mathrm{cm}^2$	4.3×10^{-6}	4.8×10^{-6}	3×10^{-7}
R_t at zero bias, $\Omega \cdot \mathrm{cm}^2$	8.4×10^{-3}	5.9×10^{-3}	1.3×10^{-2}
C_t at zero bias, F/cm^2	6.9×10^{-8}	1.5×10^{-7}	8.1×10^{-8}
τ at zero bias, s	6×10^{-10}	9×10^{-10}	1.1×10^{-9}
R_{hf} at zero bias, $\Omega \cdot \mathrm{cm}^2$	8.3×10^{-4}	1.8×10^{-3}	1.3×10^{-2}
C_{lf} at zero bias, F/cm^2	1.68×10^{-7}	2.58×10^{-7}	1.59×10^{-7}
ρ, Ω	21	14	60
$\mu, \mathrm{cm}^2 \cdot \mathrm{V}^{-1} \cdot \mathrm{s}^{-1}$	250	220	350

characteristics. The values of these parameters at zero bias are given in Table. The difference in the $I-V$ characteristics of diodes D1 and D2 is apparently due mainly to a slight difference in the composition of the solid solution of the AlGaN layer.

Symbols in Fig. 3 show the frequency dependences of the real and imaginary parts of the impedance of the test diode structures, measured at zero DC voltage bias. The resulting spectra are not described by the simplest Schottky barrier admittance model, which corresponds to an equivalent circuit with a parallel connection of frequency-independent barrier resistance R_b and capacitance C_b. It can be assumed that the reason is the impact of structural defects with trap states in the band gap of the nominally undoped GaN barrier layer. To take into account the effect of traps, we will use the simplest approach, according to which the Schottky contact can be described using the equivalent circuit shown in the inset to Fig. 3 [28,29]. The corresponding admittance per unit contact area is given by

$$g = \left[\left(\frac{1}{R_b} + i2\pi f C_b + \frac{i2\pi f C_t}{1 + i2\pi f R_t C_t} \right)^{-1} + r \right]^{-1}. \quad (4)$$

Here, i is the imaginary unit, the series circuit R_tC_t describes the trap states, r is the resistance of the non-depleted part of the barrier layer per unit area (if unintentional doping of the layer occurs). The values of the parameters of diode heterostructures at zero bias, obtained using the Φ minimization procedure, are given in Table. The corresponding model frequency dependences of Z, shown by solid lines in Fig. 3, demonstrate good agreement with experimental dependences. For comparison, the dashed lines show the model impedance spectrums in the absence of traps. The impact of traps is most pronounced in the high-barrier diode D3. The high Schottky barrier resistance of this diode does not contribute to the impedance in the frequency range under study; therefore, the real part of the impedance at frequencies less than a few gigahertzes is determined by the resistance of the traps. As follows from

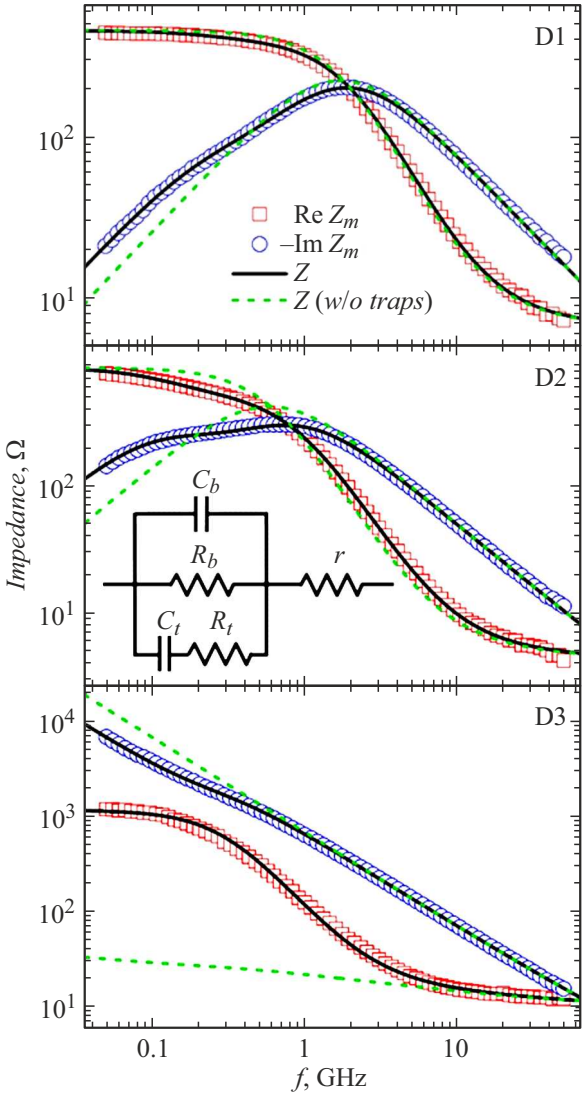

Figure 3. Experimental (symbols) and model (lines) impedance spectra of test diode structures at zero DC bias voltage. The inset shows the Schottky contact equivalent circuit used.

Table, the values of the differential resistance of the Schottky barrier of low-barrier diodes D1 and D2 obtained from the impedance spectra (R_b) are close to the corresponding static values determined from the $I-V$ characteristics (R). The values of electron mobility μ in the contact layer are calculated from the obtained values of ρ. The thicknesses l_d of the depleted regions, determined from the values of the barrier capacitance C_b, are smaller than the thickness of the barrier layer. This indicates that in the nominally undoped barrier layers there is unintentional donor doping and the layers are not completely depleted. This was confirmed by the non-zero obtained values of resistance r. In the high-barrier diode D3, the barrier layer is close to complete depletion, and r is an order of magnitude smaller than that of low-barrier diodes. When heterostructures are formed, to obtain an atomically flat growth surface, the metal-enriched mode of MBE growth of barrier layers was

used, which favors the formation of nitrogen vacancies in the semiconductor [30,31]. Therefore, it is most likely that the observed unintentional donor doping of GaN is due to nitrogen vacancies [32]. It can be seen in Table that $C_t \sim C_b$. It follows that the concentration of traps is greater than or of the order of the concentration of ionized uncompensated donors [28]. This also indicates that the nitrogen vacancies themselves can be traps. As follows from Table, the relaxation time of filling traps in diodes is $\tau = R_t C_t \sim 10^{-9}$ s. For typical cross sections of electron capture by traps in GaN, which are $10^{-16} - 10^{-13}$ cm^2, this relaxation time at room temperature corresponds to the position of trap levels 0.07–0.25 eV below the conduction band [33,28]. Structural defects with trap states in this energy range can be both nitrogen vacancies and some types of dislocations [34]. At frequencies much lower than $(2\pi\tau)^{-1}$, the diode capacitance is determined by the sum of the barrier capacitance and the trap capacitance $C_{lf} = C_b + C_t$. At frequencies much higher than $(2\pi\tau)^{-1}$, the traps almost do not contribute to the diode capacitance and reduce the diode resistance $R_{hf} = R_b R_t/(R_b + R_t)$, which improves the possibility of matching the diode with the microwave path.

Figure 4 shows the dependences of the parameters of diode heterostructures on the DC bias voltage. The obtained dependences of the barrier differential resistance of low-barrier diodes D1 and D2 are in good agreement with similar dependences determined from static $I-V$ characteristics. The barrier capacitance of low-barrier diodes first decreases with increasing reverse bias and then remains almost unchanged due to the onset of complete depletion of the barrier layer. For the same reason, with increasing reverse bias, the resistance of the non-depleted part of the barrier layer decreases and becomes zero. The barrier layer of diode D3 at zero bias is close to complete depletion; therefore, the dependence of the barrier capacitance on reverse bias is weak. It follows from Fig. 4 that with increasing reverse bias, the trap capacitance of all three diodes and the relaxation time of filling traps in low-barrier diodes decrease, which corresponds to the simplest model of traps in a Schottky contact to a uniformly doped semiconductor [28]. Another behavior of the relaxation time of filling traps under reverse bias in diode D3 ($\tau(U) \approx$ const) is due probably to complete depletion of the barrier layer and the impact of a heavily doped contact layer. Using the capacitance-voltage profiling method [33] with the found $C_b(U)$ dependences, profiles of the electron density distribution over depth in the barrier layers of low-barrier diodes were constructed. From the resulting profiles shown in Fig. 5 (square and round symbols), it follows that the concentration of ionized uncompensated donors in the barrier layers is $\sim 5 \times 10^{16}$ cm^{-3}. The sharp increase in concentration on the profiles is due to the approach of the boundary of the depleted region to the heavily doped contact layer. It is interesting to note that capacitance measurements at low frequencies can overestimate the electron/donor concentration due to

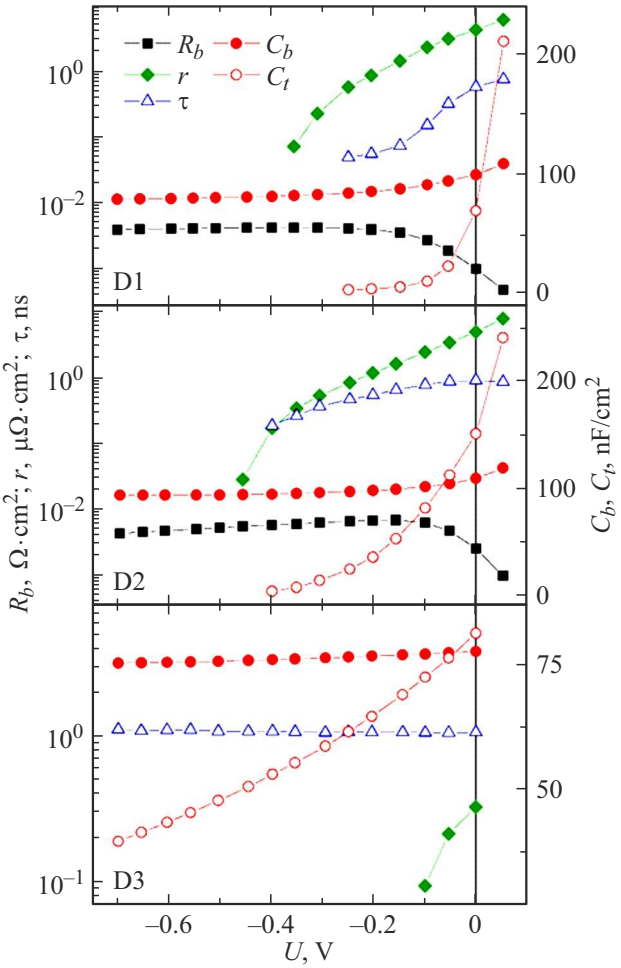

Figure 4. Dependences of the parameters of diode heterostructures on DC bias voltage.

the contribution of trap capacitance. To demonstrate this, unfilled triangular symbols in Fig. 5 show the concentration profile constructed from the capacitance-voltage dependence of the high-barrier diode heterostructure D3, which was obtained using a standard *LCR* meter at a frequency of 1 MHz based on a Schottky contact with a diameter of 200 μm, made on a separate sample. The observed concentration is overestimated by an order of magnitude. An almost identical profile (filled triangular symbols in Fig. 5) is obtained by using the sum of the found dependences of the barrier and trap capacitances on voltage $C_{lf}(U) = C_b(U) + C_t(U)$ of diode D3 to construct it.

Symbols in Fig. 6 show the experimental dependences of the volt-watt sensitivity of test diode structures on frequency. The obtained characteristics are not described by the standard frequency dependence of the volt-watt sensitivity of a Schottky diode [35]. It is expedient to assume that this is due to the presence of traps. Traps have a current nonlinearity ($R_t(U) \neq$ const), but cannot create direct current. Therefore, their effect on the volt-watt

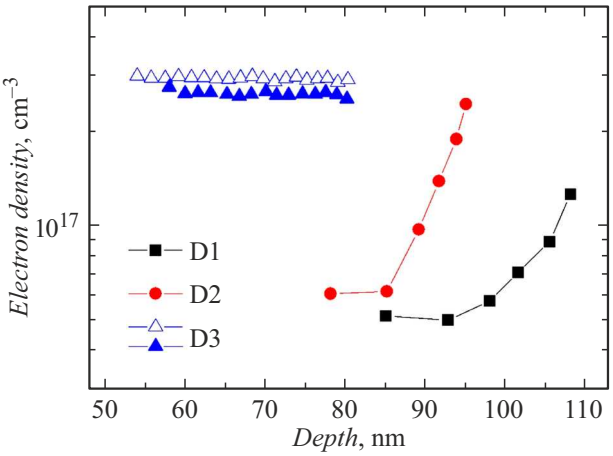

Figure 5. Profiles of the distribution of electron density over depth in the barrier layers of low-barrier D1 and D2 diode heterostructures constructed using the $C_b(U)$ dependences (square and round symbols). The electron density profile derived from the capacitance-voltage dependence of the D3 diode heterostructure obtained at a frequency of 1 MHz (unfilled triangular symbols). The electron density profile derived using the $C_{1f}(U)$ dependence of the D3 diode heterostructure (filled triangular symbols).

sensitivity is limited to additional absorption of microwave power. With this in mind, using the approach given in Ref. 35, it is easy to obtain an expression for the volt-watt sensitivity of a test diode structure with traps

$$\Re = \alpha \frac{\hat{R}_b R_1}{[r_s(0) + \hat{R}_b + R_1]\left[1 + \frac{r_s(f)}{\hat{R}_b}\right]} \times \left[1 + \frac{(2\pi f)^2 \hat{R}_b r_s(f) \hat{C}_b^{\,2}}{1 + \frac{r_s(f)}{\hat{R}_b}} \xi(f)\right]^{-1}. \quad (5)$$

Here, $\hat{R}_b = R_b/(\pi a^2)$, $\hat{C}_b = C_b \pi a^2$, R_l is the input resistance of the multimeter measuring the detected voltage (this resistance was chosen equal to 10 MΩ when low-barrier diodes D1 and D2 were measured and equal to 10 GΩ for measuring diode D3). The differences from a conventional diode are that the expression for volt-watt sensitivity (5) has an additional multiplier

$$\xi(f) = 1 + \left(\frac{C_t}{C_b}\right)^2 \frac{1 + \frac{2R_t}{R_b} + \frac{2C_b}{C_t} + \frac{\hat{R}_b}{r_s(f)}}{1 + (2\pi f R_t C_t)^2}, \quad (6)$$

related to traps, and series resistance is frequency dependent:

$$r_s(f) = \frac{r}{\pi a^2} + \frac{\rho}{8\pi} + \frac{\rho}{2\pi} \ln\left(\frac{b}{a}\right) + \mathrm{Re}[Z_e(f)]. \quad (7)$$

As can be seen from (7), series resistance consists of four terms, namely, resistance of the non- depleted part of the barrier layer under the internal contact, spreading resistance in the contact layer under the internal contact [26],

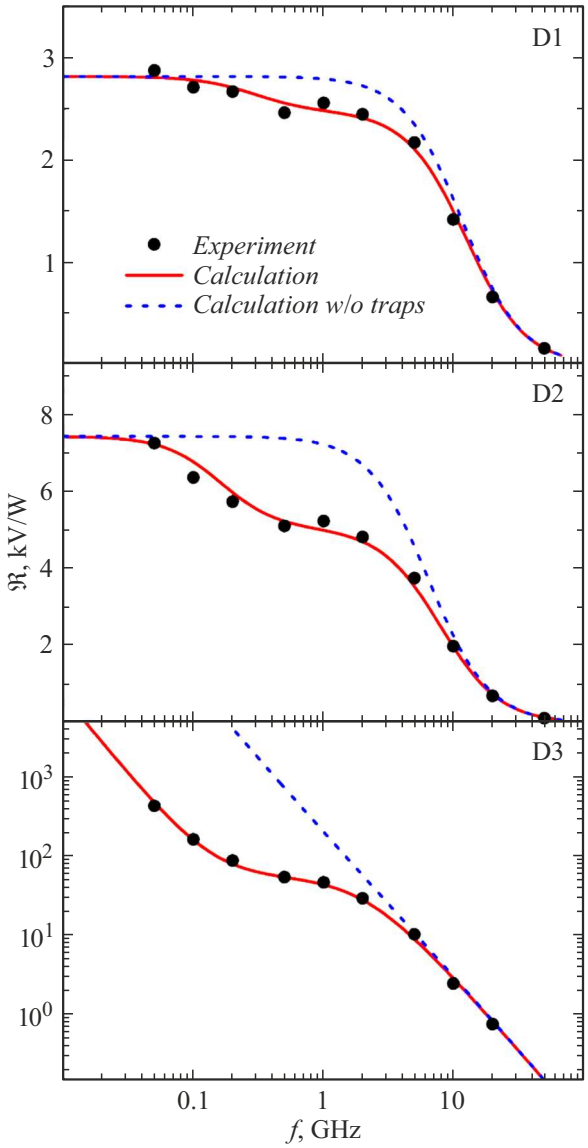

Figure 6. Experimental (symbols) and calculated (lines) dependences of the volt-watt sensitivity of test diode structures on frequency.

resistance of the annular semiconductor region between the internal and external contacts, and the real part of the external contact impedance. Calculated frequency dependences of $\Re$ shown by solid lines in Fig. 6 show good agreement with the experiment. When the calculated dependences were plotted, the low-frequency ampere-watt sensitivity α served as the fitting parameter. For diodes D1–D3, α (A/W) values 5.9, 7.5, and 13, respectively, close to those determined from static $I-V$ characteristics were obtained. The dashed lines show the dependences $\Re(f)$ that would occur without traps. It can be seen that the traps reduce the volt-watt sensitivity, but the effect is not very significant (within tens of percent) in the case of low-barrier structures. Note that the frequency dependence of the volt-watt sensitivity of the high-barrier diode structure D3 was

measured due exactly to traps that increase the microwave conductivity of the diode by several orders of magnitude, which improves its matching with the microwave path. The measurements demonstrate the possibility of using a planar low-barrier metal-semiconductor-metal structure as a sensitive detector element. This is especially true for the studied low-barrier heterostructures, where the Schottky barrier is formed in situ, which prevents the use of high-temperature thermal annealing in subsequent technological operations for the manufacture of an ohmic diode contact.

As the frequency of the detected signal increases, the volt-watt sensitivity of the diode decreases due to an increase in the shunting effect of the barrier capacitance and an increase in the fraction of microwave power dissipated by series resistance. At signal frequency f_c, called the detection cutoff frequency [35], half of the total absorbed microwave power is dissipated by series resistance and $\Re(f_c) = \Re(0)/2$. One of the ways to increase the cutoff frequency is to reduce the barrier capacitance of the detecting contact by reducing its area. Consider, using heterostructure D1 as an example, how the series resistance and cutoff frequency depend on radius a of the internal contact. Dashed lines in Fig. 7 show the calculated dependences $r_s(a)$ at $f = 0$ and $f = 100$ GHz and the dependence $f_c(a)$ for this heterostructure. At $a = 10\,\mu$m, all four terms in the expression for series resistance (7) are of the same order of magnitude and, for example, are equal to 1.4, 0.8, 2.3, and 1.1 Ω at a frequency of 100 GHz. It follows from the figures that as a decreases, series resistance increases rapidly, and the cutoff frequency, as a result, increases relatively slowly. The rapid increase in series resistance is due to the first term, namely, the resistance of the non-depleted part of the barrier layer under the internal contact, which depends quadratically on a. The second and fourth terms do not depend on a, and the third term has a weak logarithmic dependence. It follows that to optimize a diode heterostructure, it is necessary first of all to get rid of the non-depleted region in the barrier layer, i.e., pass from the Schottky contact to the Mott contact. The simplest way is to reduce the thickness of the barrier layer to a value slightly less than the thickness l_d of the depleted region. Series resistance can additionally be reduced by increasing the thickness and conductivity of the contact layer. Solid lines in Fig. 7 show the calculated dependences $r_s(a)$ and $f_c(a)$ for a hypothetical optimized diode heterostructure D1*, which has a barrier layer thickness of 75 nm, a contact-layer sheet resistance of 4.7 Ω (the layer thickness is 2 μm, the electron density is 6×10^{19} cm^{-3}, and the electron mobility is 110 cm^2·V$^{-1}\cdot s^{-1}$), and otherwise is identical to the D1 heterostructure. The electron density and electron mobility values in the contact layer used for calculations were observed in real structures with n^+-GaN layers grown in our MBE setup. It follows from the figure that a cutoff frequency of 145 GHz is reached for the D1* heterostructure at $a = 1\,\mu$m.

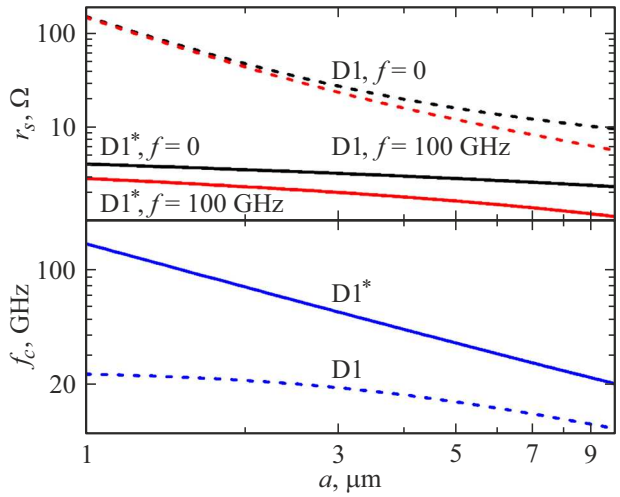

Figure 7. Calculated dependences of series resistance (at $f = 0$ and 100 GHz) and cutoff frequency on the radius of the internal contact of the test structure for the D1 diode heterostructure (dashed lines) and for the D1* hypothetical diode heterostructure with optimized parameters of the barrier and contact layers (solid lines).

3. Conclusions

Microwave properties of all-epitaxial Al/AlGaN/GaN low-barrier Schottky diodes fabricated by the MBE method have been explored. The studied low-barrier diodes had a specific differential resistance of $\sim 10^{-3}\,\Omega\cdot$cm^2 and a low-frequency ampere-watt sensitivity of about 7 A/W at zero bias. An original technique for on-wafer microwave measurements of test structures was used. All basic parameters of diode heterostructures and diode detection characteristics have been determined. It was shown that there is unintentional donor doping in the GaN barrier layer, probably by nitrogen vacancies, leading to incomplete depletion of the layer. The thickness of the depletion of the barrier layer determines the barrier capacitance, which for the studied low-lbarrier diodes had a specific value of $\sim 10^{-7}$ F/cm^2 at zero bias. The non-depleted part of the barrier layer gives the main contribution to the series resistance of small area diodes. Measurements have shown that diode heterostructures contain trap states in the semiconductor band gap with a filling relaxation time of $\sim 10^{-9}$ s. The traps observed in the barrier layer, presumably related to nitrogen vacancies or dislocations, have a notable effect on the impedance and detection properties of diodes. At frequencies much higher than the inverse of the filling relaxation time, traps increase the conductivity of the diode, which improves its matching capabilities with a microwave transmission line or antenna, but leads to a decrease in volt-watt sensitivity. The possibility of development a zero-bias microwave detector based on a planar metal-semiconductor-metal heterostructure with two back-to-back low-barrier contacts of different

areas, which does not require the formation of ohmic contact of the semiconductor with the metal, has been demonstrated. Estimates show that when optimizing the parameters of the heterostructure (reducing the thickness of the barrier layer until it is completely depleted, increasing the thickness and doping level of the contact layer), the cutoff frequency of such a detector can reach approximately 100 GHz for relevant values of the detecting contact area $\sim 10\,\mu m^2$, which is comparable to the best results.

Funding

This study was supported by the Russian Science Foundation under project No. 22-79-10029, https://rscf.ru/en/project/22-79-10029/. The equipment of the Center for Collective Use „Physics and Technology of Micro- and Nanostructures“ at the Institute for Physics of Microstructures of the Russian Academy of Sciences was used.

Conflict of interest

The authors declare that they have no conflict of interest.

References

[1] F. Sizov. Semicond. Sci. Technol., **33** (12), 123001 (2018). DOI: 10.1088/1361-6641/aae473.
[2] L.-G. Tran, H.-K. Cha, W.-T. Park. Micro Nano Syst. Lett., **5**, 14 (2017). DOI: 10.1186/s40486-017-0051-0.
[3] E.R. Brown. Solid-State Electron., **48** (10–11), 2051 (2004). DOI: 10.1016/j.sse.2004.05.074.
[4] V.I. Shashkin, Y.A. Drjagin, V.R. Zakamov, S.V. Krivov, L.M. Kukin, A.V. Murel, Y.I. Chechenin. Int. J. Infrared Milli. Waves, **28** (11), 945 (2007). DOI: 10.1007/s10762-007-9272-2.
[5] P.V. Volkov, N.V. Vostokov, A.V. Goryunov, L.M. Kukin, V.V. Parshin, E.A. Serov, V.I. Shashkin. Tech. Phys. Lett., **45** (3), 239 (2019). DOI: 10.1134/S1063785019030179.
[6] V.R. Zakamov and V.I. Shashkin. J. Commun. Technol. Electron., **56** (8), 1013 (2011). DOI: 10.1134/S1064226911060234.
[7] S.A. Korolyov, A.P. Shikov, A.V. Goryunov, V.I. Shashkin. IEEE Sensors Lett., **4** (5), 3500404 (2020). DOI: 10.1109/LSENS.2020.2986370.
[8] B. Kapilevich, V. Shashkin, B. Litvak, G. Yemini, A. Etinger, D. Hardon, Y. Pinhasi. IEEE Microw. Wirel. Compon. Lett., **26** (8), 637 (2016). DOI: 10.1109/LMWC.2016.2585557.
[9] C.H.P. Lorenz, S. Hemour, K. Wu. IEEE Trans. Microw. Theory Tech., **64** (7), 2146 (2016). DOI: 10.1109/TMTT.2016.2574848.
[10] V.T. Vo, Z. Hu. IEEE Trans. Microw. Theory Tech., **54** (11), 3836 (2006). DOI: 10.1109/TMTT.2006.884628.
[11] Z. Zhang, R. Rajavel, P. Deelman, P. Fay. IEEE Microw. Wirel. Compon. Lett., **21** (5), 267 (2011). DOI: 10.1109/LMWC.2011.2123878.
[12] P. Chahal, F. Morris, G. Frazier. IEEE Electron Device Lett., **26** (12), 894 (2005). DOI: 10.1109/LED.2005.859622.
[13] K.N. Zainul Ariffin, Y. Wang, M.R.R. Abdullah, S.G. Muttlak, O.S. Abdulwahid, J. Sexton, K.W. Ian, M.J. Kelly, M. Missous. IEEE Trans. Electron Devices, **65** (1), 64 (2018). DOI: 10.1109/TED.2017.2777803.
[14] A.C. Young, J.D. Zimmerman, E.R. Brown, A.C. Gossard. Appl. Phys. Lett., **87** (16), 163506 (2005). DOI: 10.1063/1.2112201.
[15] H. Ito, T. Ishibashi. Jpn. J. Appl. Phys., **56** (1), 014101 (2017). DOI: 10.7567/JJAP.56.014101.
[16] S. Nadar, M. Zaknoune, X. Wallart, C. Coinon, E. Peytavit, G. Ducournau, F. Gamand, M. Thirault, M. Werquin, S. Jonniau, N. Thouvenin, C. Gaquiere, N. Vellas, J.-F. Lampin. IEEE Trans. Terahertz Sci. Technol., **7** (6), 780 (2017). DOI: 10.1109/TTHZ.2017.2755503.
[17] N.V. Vostokov, M.V. Revin, V.I. Shashkin. J. Appl. Phys., **127** (4), 044503 (2020). DOI: 10.1063/1.5131737.
[18] P. Sangare, G. Ducournau, B. Grimbert, M. Faucher, C. Gaquiere. in *Proc. of the 44th European Microwave Conference* (Rome, Italy, 6–9 Oct., 2014), p. 806. DOI: 10.1109/EuMC.2014.6986557.
[19] Q. Zhou, L. Liu, X. Zhou, A. Zhang, Y. Shi, Z. Wang, Y. G. Wang, Y. Fang, Y. Lv, Z. Feng, B. Zhang. Electron. Lett., **51** (23), 1889 (2015). DOI: 10.1049/el.2015.2885.
[20] S. Regensburger, A.K. Mukherjee, H. Lu, A.C. Gossard, S. Preu, *Proc. of the 43rd International Conference on Infrared, Millimeter, and Terahertz Waves* (Nagoya, Jpn, 9–14 Sept., 2018). DOI: 10.1109/IRMMW-THz.2018.8510198.
[21] R. Quay. Gallium Nitride Electronics (Springer, 2008).
[22] *Polarization Effects in Semiconductors: From Ab Initio Theory to Device Applications*, ed. by C. Wood, D. Jena (Springer, 2008).
[23] N.V. Vostokov, M.N. Drozdov, O.I. Khrykin, P.A. Yunin, V.I. Shashkin. Appl. Phys. Lett., **116** (1), 013505 (2020). DOI: 10.1063/1.5132307.
[24] N.V. Vostokov, M.N. Drozdov, S.A. Kraev, D.N. Lobanov, A.V. Novikov, P.A. Yunin. Appl. Phys. Lett., **121** (23), 233507 (2022). DOI: 10.1063/5.0131031.
[25] N.V. Vostokov, E.A. Koblov, S.A. Korolyov, M.V. Revin, V.I. Shashkin. IEEE Trans. Electron Devices, **65** (4), 1327 (2018). DOI: 10.1109/TED.2018.2803448.
[26] J.D. Wiley. IEEE Trans. Electron Devices, **25** (11), 1317 (1978). DOI: 10.1109/T-ED.1978.19272.
[27] N.V. Vostokov, S.A. Korolev, V.I. Shashkin. Tech. Phys., **59** (7), 1036 (2014). DOI: 10.1134/S1063784214070287.
[28] J.L. Pautrat, B. Katircioglu, N. Magnea, D. Bensahel, J.C. Pfister, L. Revoil. Solid-State Electron., **23** (11), 1159 (1980). DOI: 10.1016/0038-1101(80)90028-3.
[29] W.G. Oldham, S.S. Naik. Solid-State Electron., **15** (10), 1085 (1972). DOI: 10.1016/0038-1101(72)90167-0.
[30] T. Mitsunaga, Y. Yagishita, M. Kurouchi, S. Kishimoto, J. Osaka, T. Mizutani. Phys. Stat. Sol. C, **5** (9), 3032 (2008). DOI: 10.1002/pssc.200779296.
[31] W. Kim, A.E. Botchkarev, A. Salvador, G. Popovici, H. Tang, H. Morkoc. J. Appl. Phys., **82** (1), 219 (1997). DOI: 10.1063/1.365801.
[32] J.K. Sheu, G.C. Chi. J. Phys.: Condens. Matter., **14** (22), R657 (2002). DOI: 10.1088/0953-8984/14/22/201.

[33] D.K. Schroder. *Semiconductor Material and Device Characterization*, 3rd ed. (John Wiley & Sons, Inc., Hoboken, 2006).
[34] A.Y. Polyakov, I.-H. Lee, Mat. Sci. Eng. R, **94**, 1 (2015). DOI: 10.1016/j.mser.2015.05.001.
[35] A.M. Cowley, H.O. Sorensen, IEEE Trans. Microw. Theory Tech., **14** (12), 588 (1966). DOI: 10.1109/TMTT.1966.1126337.